*Human Molecular Genetics*, 2015, Vol. 24, No. 7 1977–1990

**doi: 10.1093/hmg/ddu612**
Advance Access Publication Date: 11 December 2014
Original Article

ORIGINAL ARTICLE

# OXPHOS dysfunction regulates integrin-β1 modifications and enhances cell motility and migration

Joana B. Nunes[1,2], Joana Peixoto[1], Paula Soares[1,2], Valdemar Maximo[1,2], Sandra Carvalho[1], Salome S. Pinho[1], Andre F. Vieira[1], Joana Paredes[1,2], Ana C. Rego[4,5,6], Ildete L. Ferreira[4,6], Maria Gomez-Lazaro[3], Manuel Sobrinho-Simoes[1,2,7], Keshav K. Singh[8,9,10] and Jorge Lima[1,2,*]

[1]Institute of Molecular Pathology and Immunology of the University of Porto (IPATIMUP), Porto, Portugal, [2]Medical Faculty and [3]b.IMAGE—Bioimaging Centre for Biomaterials and Regenerative Therapies, Institute of Biomedical Engineering (INEB), University of Porto, Porto, Portugal, [4]Center for Neuroscience and Cell Biology (CNC) and [5]Faculty of Medicine, University of Coimbra—Pólo III, 3000-354 Coimbra, Portugal, [6]Institute for Interdisciplinary Research (IIIUC), University of Coimbra, 3030-789 Coimbra, Portugal, [7]Centro Hospitalar de S. João, Porto, Portugal, [8]Department of Genetics, [9]Department of Pathology and [10]Department of Environmental Health, Center for Free Radical Biology, Center for Aging and UAB Comprehensive Cancer Center, University of Alabama at Birmingham, Birmingham, Alabama and Birmingham Veterans Affairs Medical Center, Birmingham, AL 35294, USA

*To whom correspondence should be addressed at: IPATIMUP, Rua Dr Roberto Frias s/n, 4200-465 Porto, Portugal. Tel: +351 225570700; Fax: +351 225570799; Email: jlima@ipatimup.pt

## Abstract

Mitochondria are central organelles for cellular metabolism. In cancer cells, mitochondrial oxidative phosphorylation (OXPHOS) dysfunction has been shown to promote migration, invasion, metastization and apoptosis resistance. With the purpose of analysing the effects of OXPHOS dysfunction in cancer cells and the molecular players involved, we generated cybrid cell lines harbouring either wild-type (WT) or mutant mitochondrial DNA (mtDNA) [tRNAmut cybrids, which harbour the pathogenic A3243T mutation in the leucine transfer RNA gene (tRNAleu)]. tRNAmut cybrids exhibited lower oxygen consumption and higher glucose consumption and lactate production than WT cybrids. tRNAmut cybrids displayed increased motility and migration capacities, which were associated with altered integrin-β1 N-glycosylation, in particular with higher levels of β-1,6-*N*-acetylglucosamine (GlcNAc) branched *N*-glycans. This integrin-β1 N-glycosylation pattern was correlated with higher levels of membrane-bound integrin-β1 and also with increased binding to fibronectin. When cultured *in vitro*, tRNAmut cybrids presented lower growth rate than WT cybrids, however, when injected in nude mice, tRNAmut cybrids produced larger tumours and showed higher metastatic potential than WT cybrids. We conclude that mtDNA-driven OXPHOS dysfunction correlates with increased motility and migration capacities, through a mechanism that may involve the cross talk between cancer cell mitochondria and the extracellular matrix.

**Received:** October 9, 2014. **Revised and Accepted:** December 4, 2014

## Introduction

Metabolic re-wiring, or the ability to adapt cellular metabolism to growth, migration and invasion, has gained considerable attention in the cancer research field over the past decade. A cancer, by definition a proliferating and ultimately invading and metastasizing cell mass, has different nutritional demands than those of most adult tissues, which are mainly in a quiescent state (1). A key feature of the metabolic re-wiring of cancer cells is the high rate of glucose uptake to meet their increased energetic and biosynthetic needs and produce a full-blown tumour (2). Cancer cells often display the so-called 'Warburg effect', i.e. they convert most of the glucose to lactate, rather than metabolizing it through mitochondrial oxidative phosphorylation (OXPHOS), even in the presence of oxygen (3,4). This phenomenon sets mitochondrial activity, in particular OXPHOS, as a central metabolic function for tumour cells. In fact, OXPHOS activity in tumour cells is still controversial, as there are arguments supporting a deficient OXPHOS in tumourigenesis, and others agreeing with an effective utilization of OXPHOS by tumour cells (5). An increasingly accepted notion is that multiple types of tumour bioenergetic signatures occur, ranging from mainly oxidative to exclusively glycolytic, in which OXPHOS activity is significantly reduced (6).

Several mechanisms are able to induce OXPHOS downregulation in cancer, including those associated with the microenvironment (low oxygen tension) and oncogenic pathway activation [where hypoxia inducible factor-1alpha (HIF-1$\alpha$) appears as a key molecule], as well as those related to genetic alterations in OXPHOS-related genes encoded by the nuclear DNA or mitochondrial DNA (mtDNA). mtDNA mutations have been detected in a wide variety of human tumours and, in some instances, associated with poor prognosis (7–9). Such mutations are often deleterious and result in OXPHOS impairment, thereby altering mitochondrial bioenergetics and biosynthesis (10). There is compelling evidence that mtDNA mutations not only lead to OXPHOS deficiency, but also empower cancer cells with enhanced tumourigenic properties, namely increased capacity to migrate, invade and metastasize (11,12). Nonetheless, there is scant information about the molecular mechanisms and signalling pathways that connect mtDNA mutations/OXPHOS deficiency with migration, invasion and metastization. In the process of migration and invasion, cancer cells bind to molecules of the extracellular matrix (ECM) through the integrin family of transmembrane glycoprotein receptors (13). Integrins are heterodimers composed of $\alpha$ and $\beta$ subunits and mediate anchorage and migration of cancer cells over a variety of ECM molecules, such as collagen, fibronectin, laminin and vitronectin (13).

In this study, we have generated cybrid cancer cell lines that recapitulate the setting of OXPHOS deficiency (caused by a mtDNA tRNAleu mutation) and normal OXPHOS [with wild-type (WT) mtDNA]. In comparison with control cells, OXPHOS-deficient cells displayed increased motility and migration properties, which were associated with differential glycosylation and membrane localization of integrin-$\beta$1, together with increased expression of fibronectin.

## Results

### Generation of cybrid cell lines

Cybrid (cytoplasmic hybrid) cell lines are hybrid cells where the nuclear and mitochondrial genomes are from different sources (14). Cybrids are a valuable *in vitro* cellular system for the study of mitochondrial gene function, because they allow the comparison of different mtDNA genomes (either WT or mutant) against the same nuclear background.

To create cybrids with OXPHOS dysfunction (hereafter named tRNAmut cybrids), we fused mtDNA-depleted cells (143B$\rho$0 cells), which were derived from the osteosarcoma cell line 143B, with platelets harbouring the mtDNA A3243T mutation in the tRNAleu (UUR) gene, previously described as pathogenic (15). The platelets were obtained from a patient who was diagnosed with encephalomyopathy and harboured the aforementioned mutation. As controls, we used cybrids that were generated from the fusion of 143B$\rho$0 cells with WT mtDNA platelets, obtained from a healthy blood donor (hereafter named WT cybrids). The restoration of the expression of the mtDNA-encoded protein cytochrome c oxidase II (COXII) confirms that both WT and tRNAmut cybrids were successfully generated (Fig. 1A). On the other hand, 143B$\rho$o cells, which lack mtDNA, do not express COXII (Fig. 1A), but do show expression of the nuclear-encoded mitochondrial protein succinate dehydrogenase subunit A (SDHA) (Fig. 1B).

As each cell has multiple mtDNA copies, we sequenced the mtDNA to analyse the proportion of mtDNA-mutant molecules, also designated as the degree of heteroplasmy. We determined that tRNAmut cybrids display the A3243T mutation in ~50% of mtDNA molecules (Fig. 1C).

Complete mtDNA sequencing of the 143B cell line and the two cybrids confirmed the absence of mtDNA mutations in 143B and WT cybrids and that the tRNAmut cybrids only harbour the A3243T mutation in the tRNAleu (UUR) (data not shown).

### tRNAmut cybrids display decreased oxygen consumption and increased glycolytic rate than WT cybrids

After generating the WT and tRNAmut cybrids, we evaluated the metabolic changes induced by the mtDNA mutation, namely at the level of oxygen consumption (as a measure of OXPHOS function), as well as glucose consumption and lactate production (as a measure of glycolysis). As expected, 143B$\rho$o cells showed almost no oxygen consumption, while tRNAmut cybrids presented a significant decrease in basal oxygen consumption when compared with WT cybrids (Fig. 2A), confirming that the tRNA mutation leads to decreased OXPHOS function. Treatment with the complex V inhibitor oligomycin significantly decreased oxygen consumption in 143B and WT cybrids, but had no effect in 143B$\rho$0 (Fig. 2B). tRNAmut cybrids were less sensitive to oligomycin, indicating that these cells might have complex V impairment (Fig. 2B). The treatment with carbonyl cyanide 3 chlorophenylhydrazone (CCCP), which forces the mitochondria to work at its maximum respiratory capacity, increased oxygen consumption in 143B, WT cybrids and tRNAmut cybrids but not in 143B$\rho$0 (Fig. 2B).

The aforementioned differences in oxygen consumption were mirrored by the glycolytic rate of the cell lines. Glucose and lactate levels were quantified in the medium at 0 h and after 96 h of cell culture. Glucose consumption was significantly increased in 143B$\rho$0 and tRNAmut cybrids when compared with 143B and WT cybrids, respectively (Fig. 3A). Additionally, we observed that 143B$\rho$0 and tRNAmut cybrids produced more lactate when compared with 143B and WT cybrids, respectively (Fig. 3B).

The combined results of oxygen consumption, glucose consumption and lactate production suggest that the mtDNA tRNA mutation leads to OXPHOS dysfunction and a concomitant increase in glycolytic rate, a phenotype that recapitulates the Warburg effect.

It has been shown that there is a threshold for the positive tumourigenic effects of mtDNA mutations; above this threshold, there is energetic impairment that prevents tumour growth

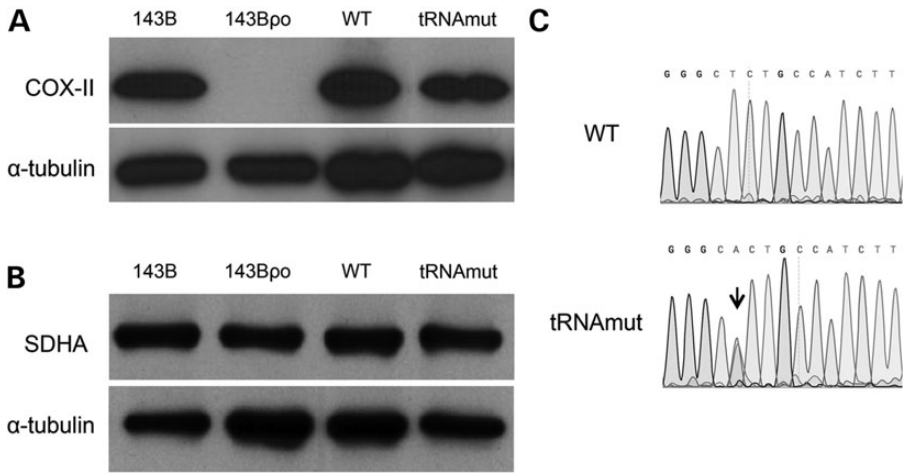


**Figure 1.** (**A**) Western blot showing that the mtDNA-encoded protein COXII is present in 143B, WT cybrids and tRNAmut cybrids, but absent in 143Bρ0; (**B**) the nuclear-encoded mitochondrial protein SDHA is present in all cell lines. (**C**) Electropherogram showing a stretch of the leucine tRNA gene in WT (top panel) and tRNAmut cybrids (lower panel) and highlighting the A3243T point mutation in the tRNAmut cybrids (arrow; electropherogram shows the reverse sequence of leucine transfer RNA gene).

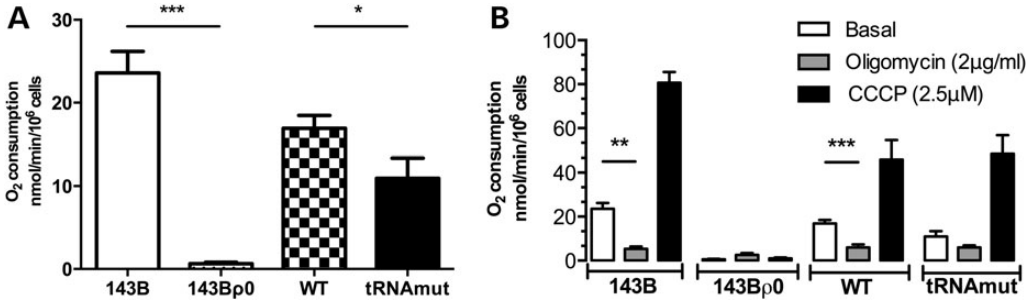


**Figure 2.** (**A**) Basal oxygen consumption in the four cell lines showing that 143Bρ0 has virtually no mitochondrial respiration and that tRNAmut cybrids have significantly less mitochondrial respiration than WT cybrids. (**B**) Sensitivity to respiration modulators: oligomycin significantly decreased oxygen consumption in 143B and WT cybrids but not in 143Bρ0 or tRNAmut cybrids. Results are representative of at least three independent experiments; error bars are SEM; $^{*}P < 0.05$; $^{**}P < 0.01$; $^{***}P < 0.001$.

(16). We thus decided to focus our analysis in the tumourigenic effects of OXPHOS dysfunction using the tRNAmut cybrids that present 50% of mutation load and compare them with 143B and WT cybrids that have normal mtDNA. Considering that complete lack of mtDNA does not occur in human tumours, 143Bρ0 cells were not further analysed.

## Cellular growth and apoptosis are decreased in tRNAmut cybrids

To address the consequences of OXPHOS dysfunction at the level of cellular growth, we counted cells over a period of 5 days and observed that tRNAmut cybrids had significantly lower growth rates than WT cybrids and 143B cells (Fig. 4A). This result indicates that, under optimal growth conditions, cells with OXPHOS deficiency have a decreased growth capacity in comparison with cells with normal OXPHOS.

Apoptosis was evaluated in the cybrid cell lines after treatment with 50 nM staurosporine (STS) [the concentration that most reflected the differences between cell lines (data not shown)]. By determining the geometric mean of the histogram, we confirmed that STS induced apoptosis in all cell lines, although this effect was only statistically significant in 143B (2-fold increase compared with untreated cells). WT cybrids showed a 1.7-fold increase compared with untreated cells, while tRNAmut cybrids were the least sensitive to STS (1.15-fold increase compared with untreated cells) (Fig. 4B and C).

## Motility and migration are increased in tRNAmut cybrids

Upon observation of the cell lines under bright field microscopy, there were evident morphological differences between the cell lines: tRNAmut cybrids presented a more spindle-like phenotype and reduced cell–cell contacts, when compared with 143B and WT cybrids (Fig. 5).

Because such morphological differences can denote different cellular migration and motility capabilities, we assessed the distance covered by single cells in the plate (motility) and the rate of closure over time in the wound-healing assay (migration) of the three cell lines, using time-lapse microscopy. In a 14 h period, tRNAmut cybrids showed significantly more individual cell motility than 143B and WT cybrids: tRNAmut cells, on average, covered ~3.3 times the distance of 143B and WT cybrids (Fig. 6A and B). In addition, the wound-healing assay showed that tRNAmut cells had the highest migratory capacity, covering 87% of the wound in 8 h, comparing with WT cybrids (43% of wound coverage) and 143B (35% of wound coverage) (Fig. 6C and D).

## tRNAmut cybrids display increased expression and binding to fibronectin

A fundamental step in cancer cell motility and migration is the interaction with the surrounding stroma. Cancer cells often secrete ECM proteins and reshape the surface expression of cell-matrix interacting molecules, such as integrins, to promote their capacity to migrate and invade the adjacent tissues (17).

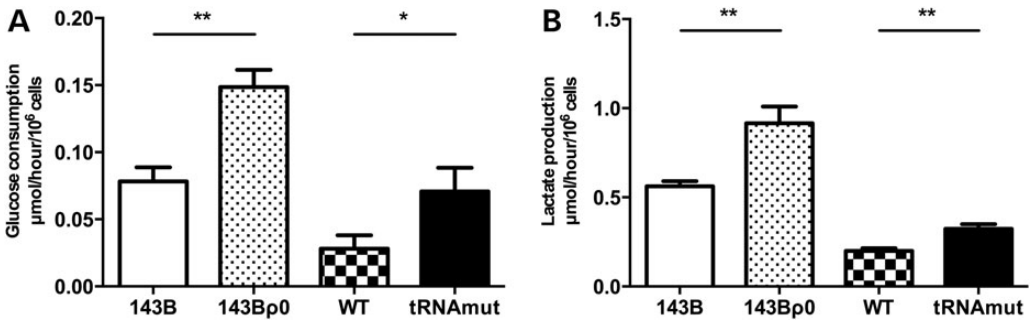


**Figure 3.** (**A**) Glucose consumption and (**B**) lactate production were assessed by quantifying glucose and lactate, respectively, in the medium of cells cultured for 96 h. Both glucose consumption and lactate production were significantly elevated in 143Bρ0 and tRNAmut cybrids when compared with 143B and WT cybrids, respectively. Results are representative of at least three independent experiments; error bars are SEM; $^{*}P < 0.05$; $^{**}P < 0.01$; $^{***}P < 0.001$.

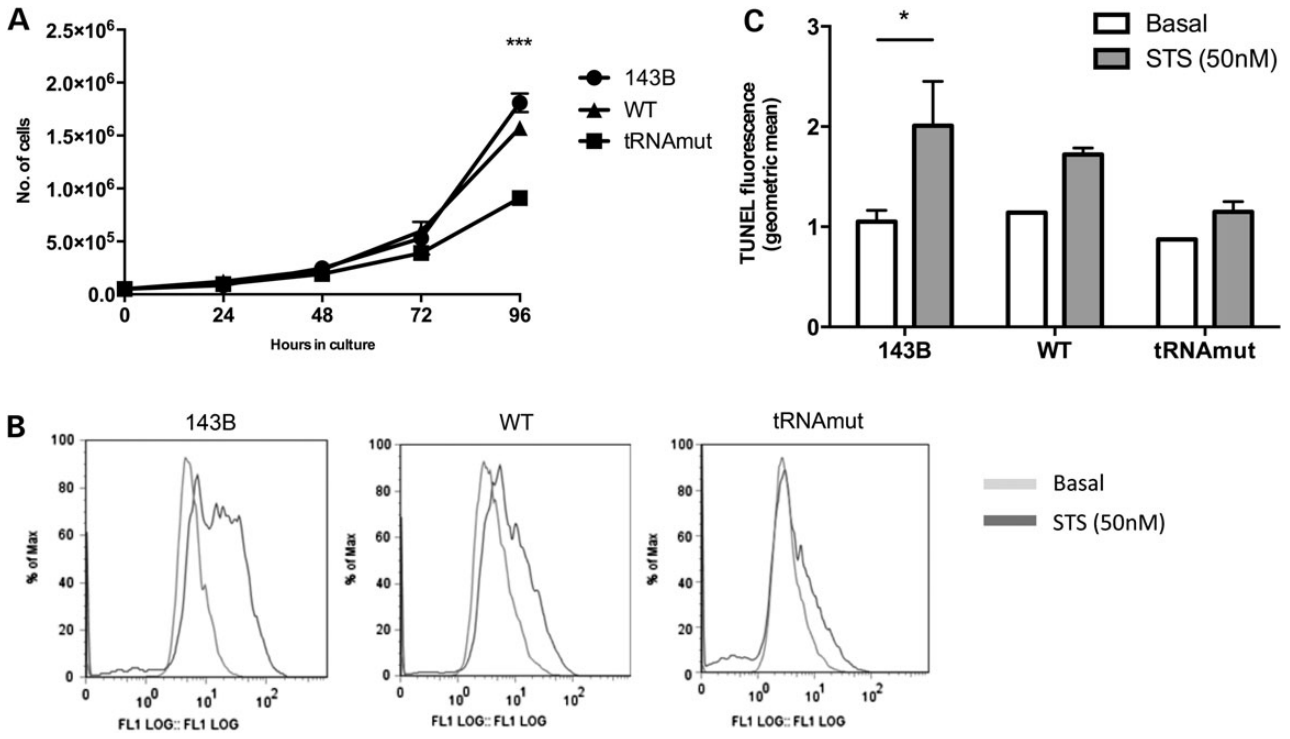


**Figure 4.** (**A**) Assessment of cell growth and (**B** and **C**) apoptosis *in vitro*. (A) In a period of 96 h, tRNAmut cells showed a slower growth rate than 143B and WT cybrids. (B) Flow cytometry analysis after incubation with 50 nM STS using terminal deoxynucleotidyl transferase dUTP nick end labeling (TUNEL). Each histogram is representative of three independent experiments. (C) Quantification of TUNEL fluorescence in untreated cells and after STS treatment: tRNAmut cybrids show the lowest response to STS. Results are representative of at least three independent experiments; error bars are SEM; $^{*}P < 0.05$; $^{**}P < 0.01$; $^{***}P < 0.001$.

To test the binding capacity to different ECM substrates, we performed an adhesion assay by culturing cells in wells coated with collagen type I, collagen type IV, fibronectin or poly-lysine (positive control). We observed that tRNAmut cybrids adhered more efficiently to fibronectin than 143B and WT cybrids (Fig. 7A), while the binding to collagen type I or IV was not significantly altered (Fig. 7B and C, respectively). Furthermore, in western-blot (WB) analysis, tRNAmut cells showed significantly increased levels of fibronectin when compared with WT cybrids and 143B (Fig. 8A and B).

## tRNAmut cybrids display increased modification of integrin-β1 with β-1,6 GlcNAc branched *N*-glycans structures

Considering that tRNAmut cybrids show higher motility, migration and binding capacity to fibronectin than 143B and WT cybrids, we addressed the status of integrin-β1 in the three cell lines. Integrins are known to play a crucial role in adhesion to the ECM, thereby contributing to migration, invasion and metastization of tumour cells (18). Integrin-β1 is one of the major players in these processes and is known to preferentially bind to fibronectin after dimerization with integrin-α5 (19).

In the WB analysis, integrin-β1 showed two distinct bands: an upper band with ~130 kDa and a lower band of ~115 kDa (Fig. 8A). Although the overall expression of integrin-β1 did not differ between the three cell lines (Fig. 8C), there was a clear difference in the relative intensity of the upper and lower band: while the parental 143B displayed similar intensity of both bands, the WT cybrids have more expression of 115 kDa integrin-β1 and tRNAmut cybrids were enriched in the 130 kDa band (Fig. 8D). In addition, the integrin-β1 130 kDa band of tRNAmut cybrids also showed less mobility in the gel than the same band of 143B and WT cybrids (Fig. 8A).

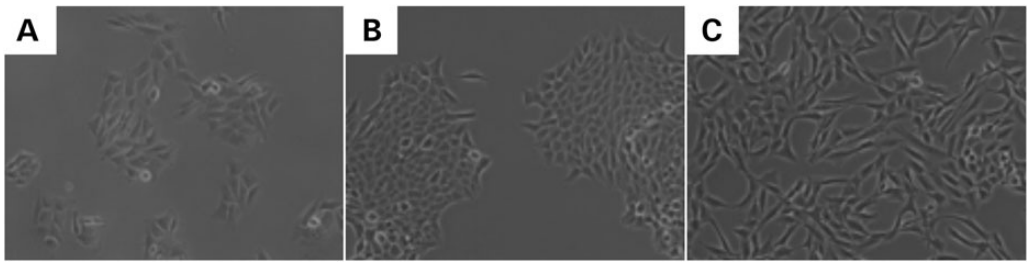


**Figure 5.** Light microscopy images of 143B (**A**), WT cybrids (**B**) and tRNAmut cybrids (**C**). The tRNAmut cybrids display reduced cell–cell contacts, showing a more spindle-like morphology than 143B and WT cybrids. Pictures were taken using the 20× objective.

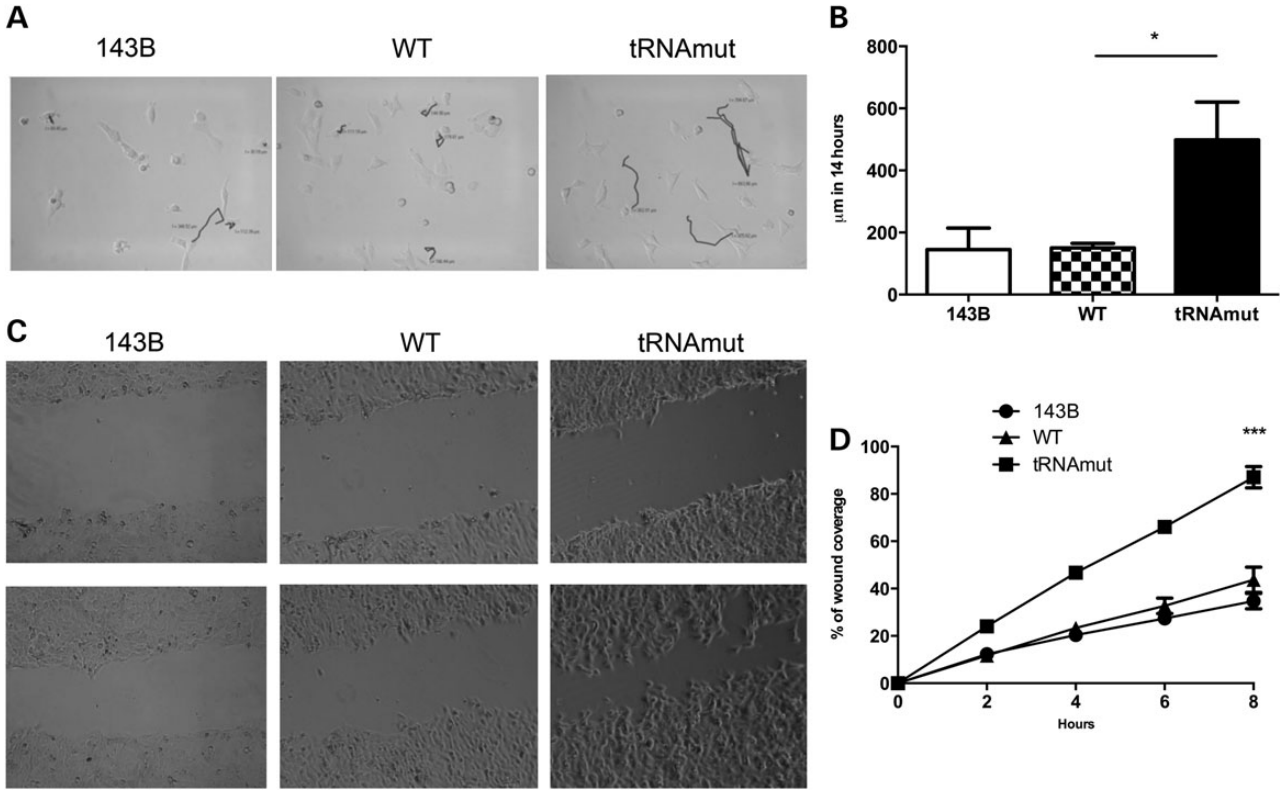


**Figure 6.** Time-lapse microscopy was used to evaluate motility (distance covered by single cells in a 14 h period; **A** and **B**) and migration (wound-healing assay in a 14 h period; **C** and **D**). In (A), the lines show the distance covered by single cells. In (C) the top panel represents the wound at baseline and the bottom panel represents the wound after 14hrs. tRNAmut cybrids showed significantly increased motility and migration when compared with 143B and WT cybrids. Each image is representative of three independent experiments. Results are representative of at least three independent experiments; error bars are SEM; $^{*}P < 0.05$; $^{**}P < 0.01$; $^{***}P < 0.001$.

Glycosylation modifications have been described to be a key regulatory mechanism of several cell biology processes, including cell adhesion and cell-matrix interaction, particularly affecting the integrin-mediated cellular migration (20,21). Taking into account that integrin-β1 is modified by N-glycosylation and that glycosylation affects the protein mobility in sodium dodecyl sulphate-polyacrylamide gel electrophoresis (SDS-PAGE) gels, we characterized the integrin-β1 N-glycosylation profile in each cybrid cancer cell lines using two different *N*-glycosidases: endoglycosidase H (Endo H), which is an endoglycosidase that cleaves within the chitobiose core of high mannose and some hybrid oligosaccharides from N-linked glycoproteins, and peptide-*N*-glycosidase F (PNGase F), which is an amidase that cleaves between the innermost GlcNAc and asparagine residues of high mannose, hybrid and complex oligosaccharides from N-linked glycoproteins. In 143B and WT cybrids, Endo H digestion completely converted the 115 kDa band to an 85 kDa band (corresponding to the size of integrin-β1 core protein), while in tRNAmut cybrids, Endo H only yielded a faint digestion product (Fig. 9A). On the other hand, PNGase F digestion converted the 130 and 115 kDa bands to the 85 kDa-sized integrin-β1 in 143B, WT cybrids and tRNAmut cybrids (Fig. 9A). These results indicate that, in 143B and WT cells, integrin-β1 is modified with high mannose, hybrid and complex type *N*-glycans, whereas in tRNAmut cybrids, integrin-β1 is mainly modified with complex type *N*-glycans. To determine whether integrin-β1 from tRNAmut cells are modified with the β-1,6 GlcNAc branched structures catalysed by beta1,6 *N*-acetylglucosaminyltransferase V (GnT-V) enzyme, we performed integrin-β1 immunoprecipitation followed by β-1,6 GlcNAc branched *N*-glycans recognition using the phaseolus vulgaris leucoagglutinin lectin (L-PHA). The increased L-PHA reactivity in tRNAmut cybrids, in comparison with 143B and WT

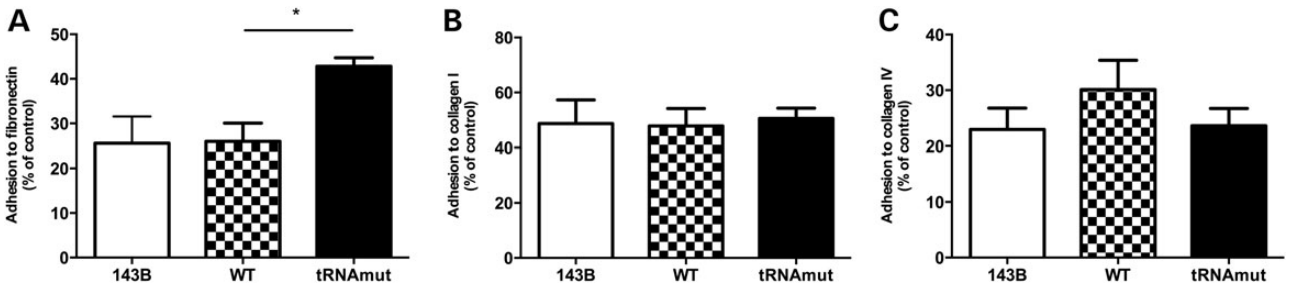


Figure 7. Quantification of cell adhesion to fibronectin (A), collagen type I (B) or collagen type IV (C), shown as percentage of adhesion to poly-lysine (positive control). tRNAmut cybrids adhere more efficiently to fibronectin than 143B or WT cybrids, while no differences were observed concerning collagen type I or type IV. Results are representative of at least three independent experiments; error bars are SEM; *$P < 0.05$; **$P < 0.01$; ***$P < 0.001$.

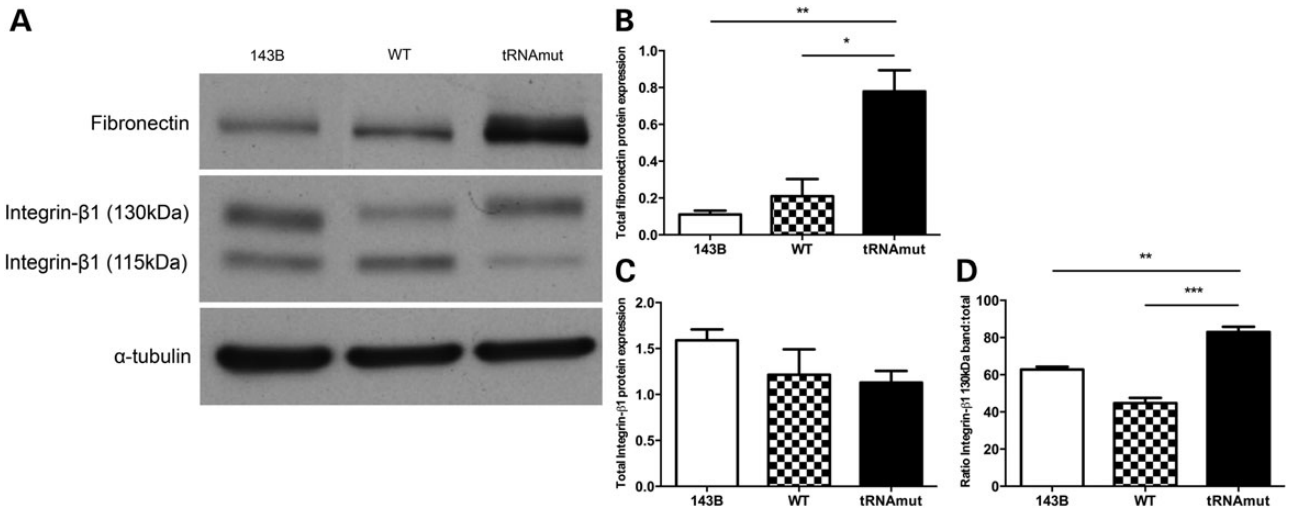


Figure 8. Western blots showing the expression of fibronectin and integrin-β1. (A) Representative WB showing increased fibronectin expression and enrichment of the integrin-β1 130 kDa in tRNAmut cybrids. The quantification of fibronectin (B), total integrin-β1 (C) and the ratio 130 : 115 kDa bands of integrin-β1 (D) is shown. Results are representative of at least three independent experiments; error bars are SEM; *$P < 0.05$; **$P < 0.01$; ***$P < 0.001$.

cells (Fig. 9B and C), demonstrates that tRNAmut cybrids are enriched in GnT-V-mediated β-1,6 GlcNAc branched structures (~3.5-fold higher than WT cybrids).

## tRNAmut cybrids show predominantly integrin-β1 and integrin-α5β1 membrane localization

We next assessed whether the differences in integrin-β1 glycosylation had an impact on its sub-cellular localization, as it had been previously shown (22). Using immunofluorescence staining, tRNAmut cybrids showed predominantly membrane-localized integrin-β1, in structures that resembled focal adhesions (Fig. 10A, upper-right picture). On the other hand, 143B and WT cybrids (Fig. 10A, upper-left and upper-middle pictures, respectively) showed mostly cytoplasmic staining. To quantify the levels of membrane-bound integrin-β1, we have used imaging flow cytometry that enables the quantification of proteins in different cellular compartments. Applying a setting that specifically quantifies the levels of membrane-localized integrin-β1, we saw that the tRNAmut cybrids displayed higher levels of membrane-bound integrin-β1 than 143B and WT cybrids (Fig. 11A). In addition, after categorizing the expression levels of membrane-bound integrin-β1 as low or high (Fig. 11E), we observed that, in the tRNAmut cybrids, the percentage of cells displaying strong expression of membrane-bound integrin-β1 was increased in comparison with 143B or WT cybrids (Fig. 11B). Conversely, 143B or WT cybrids had a higher percentage of cells displaying low expression of membrane-bound integrin-β1 than tRNAmut cybrids (Fig. 11B).

Because integrin-β1 requires dimerization with α subunits for proper function, we have used the same imaging flow cytometry analysis to quantify the levels of membrane-bound integrin-α5β1, the dimer that preferentially binds fibronectin. Similarly to what we observed for integrin-β1, the levels of membrane-bound integrin-α5β1 were elevated in tRNAmut cybrids, when compared with 143B and WT cybrids (Fig. 11C). tRNAmut cybrids also showed a higher percentage of cells with a higher expression of membrane-bound integrin-α5β1 and lower percentage of cells with low expression, when compared with 143B and WT cybrids (Fig. 11D).

## Phenformin, a complex I inhibitor, mimics the effects of the tRNA mutation

Phenformin is a selective OXPHOS complex I inhibitor (23). We have tested the effects of phenformin in WT cybrids and found that it inhibited $O_2$ consumption to a degree similar to that of oligomycin (Fig. 10C). To evaluate whether phenformin-induced OXPHOS dysfunction in 143B and WT cybrids had an impact on integrin-β1 localization, we treated cells with 5 mM of phenformin for 1 h and evaluated the effects by confocal microscopy and imaging flow cytometry. Using

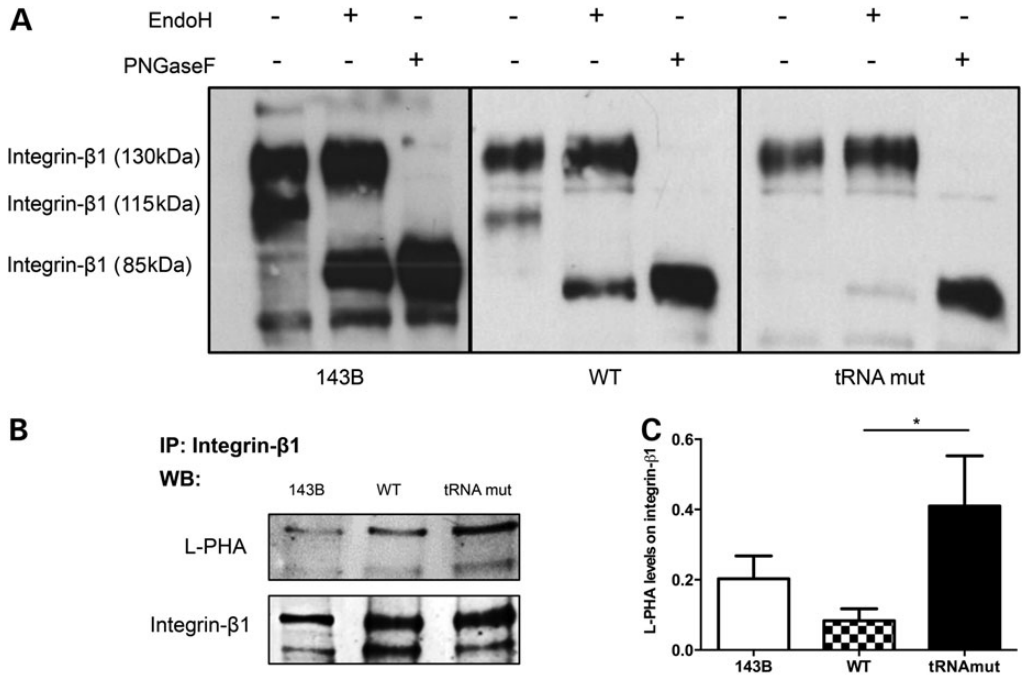


**Figure 9.** (**A**) Sensitivity to the glycan-cleaving enzymes Endo H (cleaving only high-mannose type glycans) and PNGase F (cleaves all N-linked glycans). 143B and WT, but not tRNAmut cybrids were sensitive to treatment with Endo H, while all cell lines were sensitive to PNGase F. (**B**) Integrin-β1 immunoprecipitation followed by β-1,6 GlcNAc branched *N*-glycans recognition (using L-PHA lectin). tRNAmut cybrids show significantly increased levels of β-1,6 GlcNAc branched *N*-glycan structures in integrin-β1 in comparison to WT cybrids (**C**). Results are representative of at least three independent experiments; error bars are SEM; $^{*}P < 0.05$; $^{**}P < 0.01$; $^{***}P < 0.001$.

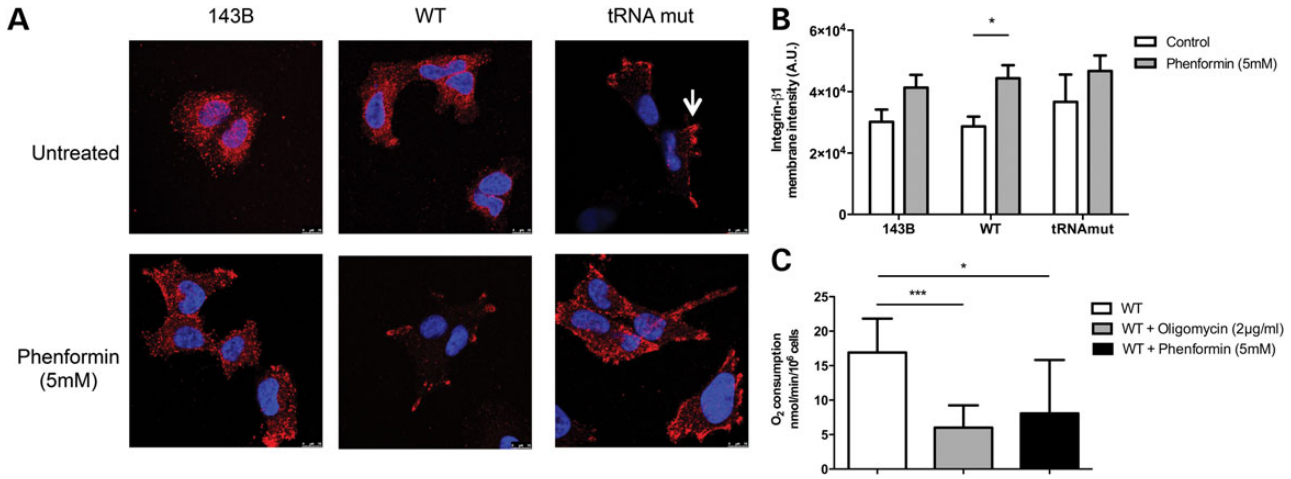


**Figure 10.** (**A**) Confocal microscopy using anti-integrin-β1 antibody (red). Untreated 143B and WT cells displayed integrin-β1 expression mainly localized in the cytoplasm, while tRNAmut cybrids showed integrin-β1 mainly in membrane protrusions, in structures that resembled focal adhesions (arrow). Further, 5 mM phenformin treatment in 143B and WT cybrids induced an integrin-β1 expression pattern that mimicked that found in untreated tRNAmut cybrids. Nuclei are stained in blue [4',6-diamidino-2-phenylindole]. Pictures were taken using the 63× objective. (**B**) Quantification of membrane-bound integrin-β1 by imaging flow cytometry in cells treated with 5 mM phenformin, showing that the levels of membrane-bound integrin-β1 increase in all cell lines, although only significantly in WT cybrids. (**C**) Phenformin treatment significantly reduces oxygen consumption in WT cybrids. Results are representative of at least three independent experiments; error bars are SEM; $^{*}P < 0.05$; $^{**}P < 0.01$; $^{***}P < 0.001$.

confocal microscopy, 143B and WT cybrids showed membrane re-localization of integrin-β1 with a pattern that closely resembled that of tRNAmut cybrids, whereas phenformin had little effect on integrin-β1 localization in tRNAmut cybrids (Fig. 10A, bottom panels). After quantification by imaging flow cytometry, we confirmed that phenformin increased the levels of membrane-localized integrin-β1 in all cell lines, although only reaching the level of statistical significance in WT cybrids (Fig. 10B). Such effect was less evident in the tRNAmut cybrids that intrinsically have OXPHOS dysfunction and present higher levels of membrane-bound integrin-β1 (Fig. 10B).

## tRNAmut cybrids have higher tumourigenic potential in nude mice than WT cybrids

Taking into consideration that a metabolic defect might have considerably different effects depending on the microenvironment, we assessed the tumour-forming capacity of WT and tRNAmut cybrids *in vivo*. One million cells were injected in the

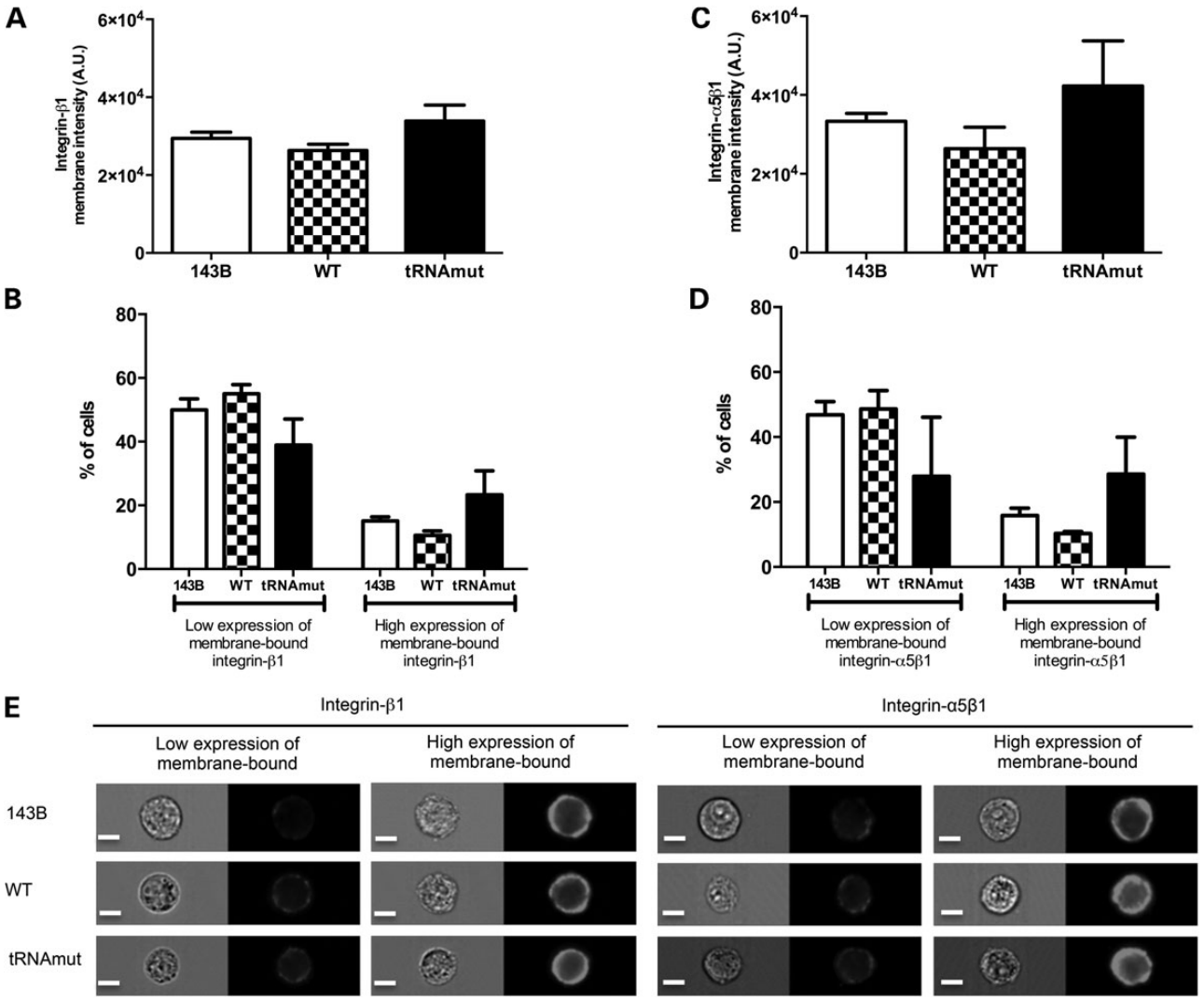


**Figure 11.** Imaging flow cytometry quantification of the membrane-bound integrin-β1 and membrane-bound integrin-α5β1. Graphics (**A**) and (**C**) illustrate the mean expression level of membrane-bound integrin-β1 and membrane-bound integrin-α5β1, which are increased in tRNAmut cybrids when compared with 143B and WT cybrids. In graphics (**B**) and (**D**), we sub-divided the cell population into those with low or those with high expression of membrane-bound integrin-β1 or integrin-α5β1. tRNAmut cybrids have an increased proportion of cells with high expression levels of membrane-bound integrin-β1 (B) and integrin-α5β1 (D); conversely, 143B and WT cybrids have increased percentage of cells with low levels of membrane-bound integrin-β1 (B) and integrin-α5β1 (D). Results are representative of at least three independent experiments; error bars are SEM. For the three cell lines, representative bright-field images and the corresponding fluorescent image from the low or high expression membrane-bound integrin-β1 or integrin-α5β1 cell populations acquired with the imaging flow cytometer are shown in (**E**). Scale bar 10 μm.

dorsal flank of nude mice and tumour growth was monitored for ~36 days. While tumour formation was observed in all mice injected either with WT or with tRNAmut cybrid cells (except one mouse injected with the WT cybrid), the tumours derived from tRNAmut cybrids were significantly larger in volume than tumours derived from WT cybrids (Fig. 12A). In addition, we observed metastatic foci in the lungs of 3 of the 14 mice injected with tRNAmut cybrids, while no animal injected with WT cybrids had lung metastases (data not shown). To further assess the metastatic potential of WT and tRNAmut cybrids, we repeated the *in vivo* tumour-forming capacity experiment, but instead of sacrificing the animals by Day 36, the tumours were removed and the mice were kept alive until Day 49 (13 days after tumour removal) to allow the formation of metastases. After collecting the lungs of the animals, we performed immunohistochemistry against vimentin (a marker expressed by WT and tRNAmut cybrids) and found that 67% of mice injected with tRNAmut cybrids displayed lung metastases, whereas only 33% of mice injected with WT cybrids had lung metastases (Fig. 12B and C).

## Discussion

In his seminal works, Warburg postulated that deficient OXPHOS was on the origin of tumourigenesis, owing to his consistent observations of lack of respiration and increased lactate production in human tumours (3). Because this phenotype persisted even in the presence of oxygen, Warburg designated it as aerobic glycolysis. Several lines of evidence have confirmed that OXPHOS deficiency is common to many human tumours, although its functional role in tumour development remains under study.

The consequences of mitochondrial OXPHOS dysfunction in cancer cells have been addressed by various approaches, namely chemical inhibition (using OXPHOS-targeted drugs, such as oligomycin, rotenone or phenformin) or genetic manipulation, via

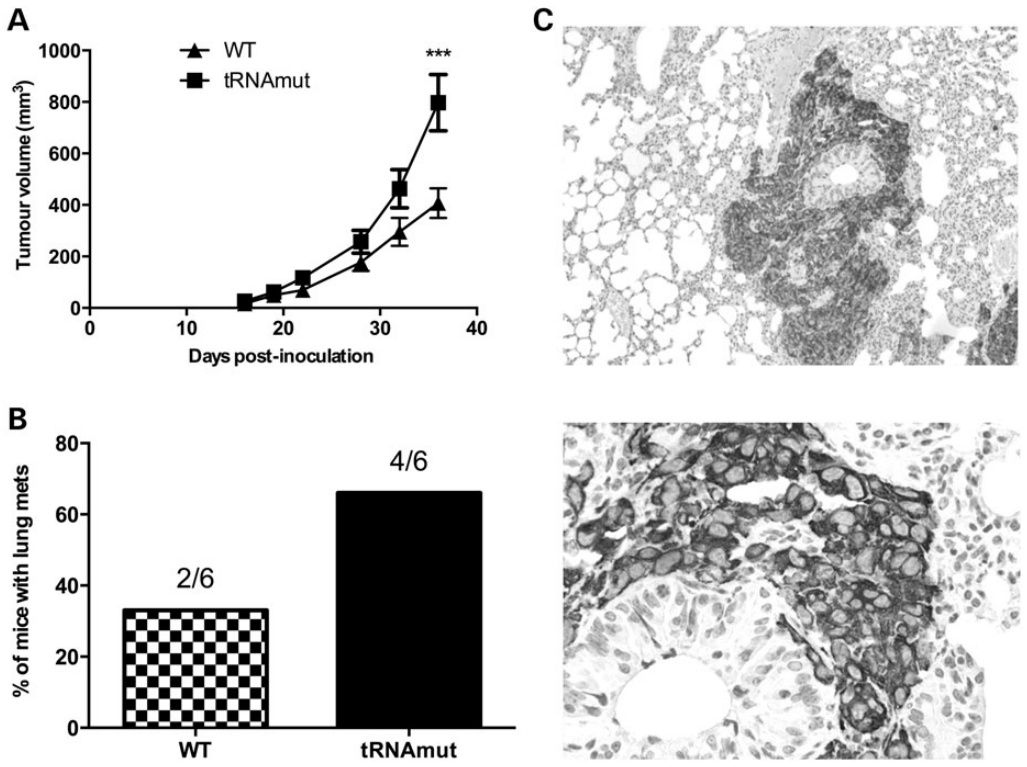


**Figure 12.** *In vivo* tumour growth and metastatic capacity of WT and tRNAmut cybrids. After injecting in the dorsal flank of nude mice, tRNAmut cybrids gave rise to larger tumours than WT cybrids (**A**). Metastatic potential (**B**) was assessed by injecting cells in the dorsal flank of nude mice, removing the tumours (~Day 36) and euthanizing mice by Day 49. The analysis of the whole lungs revealed that 67% of the animals injected with tRNAmut cells presented lung metastases, while only 33% of those injected with WT cybrids showed lung metastases. (**C**) Illustration of a lung metastasis in an animal injected with tRNAmut cybrids. Pictures were taken using the 10× objective (top image) and the 40× objective (bottom image).

the introduction of mtDNA mutations (cybrid cell lines). mtDNA mutations are found in a wide variety of cancers, such as colorectal, thyroid, gastric, breast, leukaemia, glioblastoma and prostate (10,24–28). Many of such mutations are deleterious and able to inhibit OXPHOS, implying that alterations in mitochondrial bioenergetics and metabolism have a role in supporting neoplastic transformation. An interesting finding is that there is no mutational hotspot within mtDNA; instead, mtDNA mutations are scattered across the mitochondrial genome, spanning all the OXPHOS-encoding genes, suggesting that the key target is OXPHOS function, rather than a specific gene.

Following the genetic-based strategy, we created a cybrid cell model, where we engineered cells to have WT mtDNA (WT cybrids) or a pathogenic mtDNA mutation (tRNAmut cybrids). Given the diversity of mtDNA mutations found in human cancers, we chose to use a deleterious mutation (A3243T in the leucine tRNA) that clearly induces OXPHOS dysfunction (15). In this way, our model is well fitted to address the converging outcome of mtDNA mutations, i.e. OXPHOS dysfunction. In addition, this mutation occurs in the same nucleotide as the A3243G, which has already been detected in human cancers (29,30). Our results showed that tRNAmut cybrids exhibited OXPHOS dysfunction, because they display lower oxygen consumption when compared with WT cybrids. This is in line with a previous report showing that the same germline mutation caused decreased activity of complexes I, III and IV in the muscle fibres of an encephalomyopathy patient (15). Furthermore, tRNAmut cybrids showed a metabolic shift towards aerobic glycolysis, as evidenced by the increased glucose consumption and lactate production. This cybrid model thus constitutes a valuable tool to study the phenotypic effects of OXPHOS dysfunction.

The influence of the microenvironment over tumour cell behaviour is an important aspect for studying the relevance of altered metabolism in tumourigenesis. When we compared growth capacity *in vitro*, tRNAmut cybrids showed slower growth rate than WT cybrids. However, when injected in the dorsal flank of nude mice, tRNAmut cybrids produced larger and faster-growing tumours. These results are in accordance with previous studies using cybrid cells (31–33) and fit with numerous examples where the *in vivo* results diverge from the results obtained *in vitro*. It is possible that, within the microenvironment where the cells are injected, the nutrient availability, presence of fibroblasts and immune cells may provide growth advantage to OXPHOS-deficient cells, while optimal *in vitro* growth conditions benefit OXPHOS-proficient cells. Moreover, tRNAmut cybrids seem to be more resistant to the apoptosis inducer STS, a finding that could also explain the increased size of the tumours produced by tRNAmut cybrids in nude mice. Several studies showed that mtDNA mutations suppress apoptosis in cultured cybrids (32,33), which is in accordance to the crucial role played by mitochondria and the respiratory chain in apoptosis (34).

WT and tRNAmut cybrids showed marked differences concerning motility and migration: tRNAmut cybrids displayed higher individual cell motility (when plated in low density) and migration (wound healing) than WT cybrids. These differences were associated with distinct cell morphology: WT cybrids formed colonies with clear cell–cell interactions, whereas tRNAmut cybrids appeared as individualized (dispersed) cells with few cell–cell

contacts. Noteworthily, when injected in nude mice, tRNAmut cybrids produced more lung metastases than WT cybrids, suggesting that the *in vitro* migratory capacities of tRNAmut cybrids were associated with an increased metastatic ability *in vivo*.

Our results fit with previous findings suggesting that OXPHOS dysfunction increases the migratory and metastatic potential of cancer cells (11,12,33). In some of these studies, reactive oxygen species (ROS) were pointed out as important mediators of the enhanced migration and metastization of OXPHOS-deficient tumour cells (12), although the underlying effector molecules remain to be clarified.

OXPHOS dysfunction has been advanced to modulate the ECM in a way that promotes cell invasion and metastatic properties (35,36). Crucial for migration and invasion, the crosstalk cancer cell-stroma is mediated by adhesion proteins, where integrins play a central role by regulating a diverse array of cellular functions necessary to the initiation, progression and metastization of solid tumours (18). Surface integrin-β1 promotes cell migration and invasion by binding to fibronectin in the ECM. In our experiments, tRNAmut cybrids showed both an increased expression and binding to fibronectin compared with 143B and WT cybrids. Interestingly, while no significant changes were observed in the total levels of integrin-β1, tRNAmut cybrids consistently exhibited higher levels of the 130 kDa integrin-β1 isoform than 143B and WT cells.

Integrins are glycoproteins and therefore major carriers of *N*-glycans (sequences of carbohydrates attached to asparagine residues of the protein). Glycosylation has been described as a fundamental molecular mechanism affecting the folding, expression, intracellular trafficking, localization, activity and half-life of several proteins, both in normal and pathological conditions (37,38). Integrin-β1 is tightly regulated by N-glycosylation. Indeed, deglycosylation mutants of integrin-β1, or treatment with the N-glycosylation inhibitor tunicamycin, abolish integrin-β1 transport to the cell surface and its binding to ECM substrates (21). Moreover, aberrant N-glycosylation with increased expression of β-1,6 GlcNAc branched *N*-glycans (catalysed by GnTV enzyme) directs more integrin-β1 delivery to plasma membrane and promotes fibronectin-based cell migration and invasion (39). Such β-1,6 GlcNAc branched glycans in integrin-α5β1 have been shown to be associated with increased cell spreading on fibronectin in a context of oncogenic signalling driven by mutant Ras (40).

Our results show that integrin-β1 N-glycosylation pattern differs between WT and tRNAmut cybrids, specifically in the levels of integrin-β1 modified with the β-1,6 GlcNAc branched *N*-glycans that were significantly elevated in tRNAmut cybrids. In line with previous reports (39,40), such integrin-β1 N-glycan modification in tRNAmut cybrids may account for their increased binding to fibronectin, as well as for enhanced motility and migration capabilities.

Our observation of differential integrin-β1 N-glycosylation levels between tRNAmut and WT cybrids may be associated with (i) increased expression or enzymatic activity of GnT-V or (ii) increased availability of the substrates for N-glycosylation such as UDP-N-acetylglucosamine (UDP-GlcNAc), promoting an increased N-glycosylation biosynthetic pathway. The production of UDP-GlcNAc for N-glycosylation is achieved by the hexosamine biosynthetic pathway, which requires the coordination of both glucose and glutamine metabolism. Indeed, UDP-GlcNAc levels have been shown to be critical factors in the production of β-1,6-branched *N*-glycans, as they increase the production of these sugar chains without an increase in GnT-V activity (41). While our data associate OXPHOS deficiency to increased glucose uptake, it has also been observed that glutamine metabolism is essential for cancer cells harbouring mtDNA mutations (42). Taking all this together, we speculate that OXPHOS deficiency may remodel glucose and glutamine metabolism, thereby affecting the intracellular pool of N-glycosylation substrates and leading to the modification of the N-linked glycosylation of membrane proteins like integrin-β1. Interestingly, Wellen *et al.* (43) demonstrated that glucose availability to the hexosamine pathway regulates interleukin-3 receptor alpha (IL-3Rα) surface expression in a N-linked glycosylation-dependent manner. Our finding on the association between carbohydrate maturation on integrin-β1 and the glycolytic shift caused by OXPHOS deficiency thus support and extend the results of Wellen *et al.* (43), strengthening the notion that cellular metabolism can affect signal transduction through regulation of glycosylation.

Hung *et al.* (44) had advanced a connection between OXPHOS deficiency and integrin signalling in a model of gastric cancer cells. Hung *et al.* (44) used a model of chemically induced OXPHOS dysfunction (using the mitochondrial inhibitors oligomycin and antimycin A) and proposed that mitochondrial dysfunction enhances migration through mitochondria-generated ROS-mediated integrin-β5 expression. We focussed mainly on the effects elicited by genetically induced OXPHOS dysfunction, but we also observed that treatment with the mitochondrial complex I inhibitor phenformin resulted in increased surface expression of integrin-β1. Our results, combined with those of Hung *et al.* (44), suggest that mitochondrial dysfunction is associated with integrin-mediated cell motility, migration and invasion.

In conclusion, we have built an *in vitro* cybrid cell model that recapitulates OXPHOS dysfunction of tumour cells induced by mtDNA mutations. In this study, we show that OXPHOS dysfunction has a major impact in the migratory phenotype of cancer cells *in vitro*, and that the adhesion glycoprotein integrin-β1 may be behind the mechanism by which the defect in OXPHOS leads to an increased motility and migration capacity. In addition, when transplanted in nude mice, tRNAmut cybrids display increased tumourigenic/metastatic potential than WT cybrids.

## Materials and Methods

### Cell lines

Cell lines were cultured in Dulbecco's modified Eagle's medium high-glucose supplemented with 10% (v/v) inactivated foetal bovine serum (FBS), 100 units/ml penicillin, 100 μg/ml streptomycin (all from GIBCO, Life Technologies, NY, USA) and 50 μg/ml uridine (Sigma-Aldrich, St. Louis, USA). Cells were maintained at 37°C, 5% $CO_2$ in a humidified incubator and cultured as a monolayer.

The 143Bρ0 is an mtDNA-depleted cell line, derived from 143B osteosarcoma cells after transient expression of UL12.5 *Herpes simplex* protein (45). Compared with the alternative method of generating ρ0 cells—long-term exposure to ethidium bromide—this method of mtDNA depletion has the advantage of selective degradation, assuring that no alterations are induced in the nuclear DNA.

Cybrid cell lines were obtained after fusion of 143Bρ0 cells with human platelets harbouring either WT or mutant mtDNA. Platelets were isolated from peripheral blood collected in ethylenediaminetetraacetic acid (EDTA) tubes. Whole blood was mixed with one-tenth (v/v) of a 10× warm salt solution of citrate (0.15 M NaCl and 0.1 M trisodium citrate dehydrated, pH 7.0), and centrifuged for 20 min at 200*g*. To pellet the platelets, the top three-fourths of the platelet-rich plasma (supernatant) were centrifuged for 20 min at 1500*g*. Platelets were resuspended in

physiological saline (0.15 M NaCl, 15 mM Tris–HCl, pH 7.4) as previously described (46).

After isolation, the platelet suspension was centrifuged for 15 min at 1500*g* and the supernatant discharged. One million 143Bρ0 cells were carefully added to the platelets' pellet, which was then centrifuged for 10 min at 180*g*. The cellular fusion was achieved when the pellet was resuspended in 0.1 ml of PEG 45% (v/v) and incubated for 1 min. The fusion mixture was then plated in Petri dishes in different dilutions (1 : 1, 1 : 10 and 1 : 100) and selection began 48 h later, by removing uridine from the culture medium. Only the clones that survive and proliferate after uridine removal were selected.

### Western blot analysis

Cells were detached with Versene dissociation solution (GIBCO) and lysed in RIPA buffer (50 mM Tris–HCl, 1% NP-40, 15 mM NaCl and 2 mM EDTA, pH 7.5) supplemented with protease (Roche Applied Science, Penzberg, Germany) and phosphatase inhibitors (Sigma-Aldrich). Protein extracts (25–100 μg) were denatured, resolved in SDS-PAGE gels and then electrotransferred onto a nitrocellulose membrane (GE Healthcare, Piscataway, USA) for 2 h at 100 V and 4°C, or alternatively overnight at 30 V and 4°C.

Membranes were blocked for 1 h at room temperature [in phosphate buffered saline (PBS) containing 0.5% Tween-20 and 5% low-fat dry milk] and incubated with primary antibodies diluted in blocking solution, according to the manufacturer's instructions. The primary antibodies used were the following: α-tubulin (Sigma-Aldrich); COXII (Mitosciences, Abcam, Cambridge, UK); SDHA (Mitosciences); fibronectin (Santa Cruz, Dallas, USA); integrin-β1 (BD Transduction Laboratories, San Jose, USA). Membranes were then washed with PBS-T and incubated with the suitable horseradish peroxidase conjugated secondary antibody. Protein bands were detected by chemiluminescense and X-ray film exposure (GE Healthcare).

### Measurement of oxygen consumption

Cells were trypsinized and resuspended in FBS-containing culture medium. Cells were counted and aliquots containing $5 \times 10^6$ cells were further pelleted, resuspended in Krebs buffer containing 132 mM NaCl, 4 mM KCl, 1 mM $CaCl_2$, 1.2 mM $NaH_2PO_4$, 1.4 mM $MgCl_2$, 6 mM glucose and 10 mM 4-(2-hydroxyethyl)-1-piperazineethanesulfonic acid and allowed to equilibrate for 5 min in an oxygen electrode chamber (DW1, Clark electrode, Hansatech, Norfolk, UK), after calibration for dissolved oxygen. After recording the basal rate of oxygen consumption (in nmol/ml/min), maximum respiration was assessed by adding 2.5 μM CCCP plus 2 μg/ml oligomycin to the reaction medium. Potassium cyanide (700 μM) was added at the end of the experiment to confirm $O_2$ consumption by mitochondria.

### Glucose and lactate quantification

Identical cell numbers ($10^4$) were plated in 6-well plates and the medium was collected at 0 h and after 96 h in culture. Glucose levels present in the conditioned medium after 96 h in culture were quantified using the Glucose GOD/PAP Kit (Roche Applied Science) and subtracted to the initial levels (0 h). Lactate was quantified in a similar manner, using the lactic oxidase-peroxidase (LO-POD) enzymatic colorimetric assay (Spinreact, Sant Esteve de Bas, Spain).

### Cell population growth and apoptosis

For cell population growth studies, identical cell numbers ($10^4$) were plated in 6-well plates and cells were counted in 24 h intervals, for 96 h, using a Z Series Particle Count and Size Analyser (Beckman Coulter, Brea, USA).

The terminal deoxynucleotidyl transferase dUTP nick end labeling (TUNEL) assay ['*In situ* cell death detection kit, fluorescein' (Roche Applied Science)] was used to evaluate and quantify apoptosis induced by STS. Cells were treated for 4 h with three concentrations—25, 50 and 100 nM—of STS in dimethyl sulfoxide and the assay was performed according to the manufacturer's protocol. The fluorescence was detected in the range of 515–565 nm by flow cytometry (Beckman Coulter). Analysis of the results was performed in FlowJo software (Tree Star) and the geometric mean of the curves was calculated. Whenever necessary, a gate was drawn to exclude unspecific fluorescence.

### Motility and migration

For individual motility assays, cells were plated in low density ($10^4$ cells) in a 12-well plate. After seeding for 24 h, cells were monitored for 14 h using a Leica DMI 6000B time-lapse microscope (Leica Microsystems, Wetzlar, Germany). The movement covered by a single cell was quantified only if the cell was clearly individualized, remained in the field and did not enter division or apoptosis. For migration (wound healing) assays, cells were plated in high density ($5 \times 10^5$ cells), to reach confluence. After seeding for 8 h, the cell monolayer was scratched with a pipette tip, cell debris was removed by replacing the culture medium and cells were monitored in a Leica DMI 6000B time-lapse microscope (Leica Microsystems) using the 10× objective. Migration was defined as the capacity to migrate into the wound and measured as the percentage of wound coverage through time. For both assays, images were automatically collected in each field every 5 min using LAS AF software (Leica Microsystems) and further processed using the same software. Appropriate groups of images corresponding to the same field were joined to make the film.

### PNGase F and Endo H digestion

Total cell lysates (30 μg) were combined with denaturing buffer and incubated at 100°C for 10 min. Samples were then digested with 1 unit of PNGase F or Endo H (New England Biolabs, Ipswich, USA) overnight at 37°C. The deglycosylated proteins were loaded in SDS-PAGE gels and immunoblotted with anti-integrin-β1 antibody (BD Transduction Laboratories). For controls, samples were incubated without the enzymes.

### Integrin-β1 immunoprecipitation and lectin blot analysis

Equal amounts of total protein (1500 μg) from each cell lysate were pre-cleared with protein G-sepharose beads (GE Healthcare) for 1 h and the supernatant was incubated overnight with 5 μg of monoclonal antibody against integrin-β1 (BD Transduction Laboratories). After that, incubation with protein G-sepharose for 2 h was performed and the immune complexes were released by boiling for 5 min at 95°C in Laemmli buffer. Protein extracts were resolved in SDS-PAGE gels, electrotransferred onto a nitrocellulose membrane (GE Healthcare) for 2 h at 100 V and then probed with the primary antibody against integrin-β1 (BD Transduction Laboratories). For β-1,6 GlcNAc branched structure analysis on integrin-β1 immuno-precipitated, membranes were probed with biotinylated *Phaseolus vulgaris* leucoagglutinin lectin

(L-PHA), a lectin that specifically recognizes the β-1,6 GlcNAc branched N-glycan structure catalysed by *N*-acetylglucosaminyltransferase V (Vector Laboratories, Burlingame, USA). Protein bands were detected by chemiluminescense and X-ray film exposure (GE Healthcare).

### Confocal microscopy

Cells were seeded on top of glass coverslips, fixed with 4% paraformaldehyde, permeabilized with 0.1% Triton X-100, blocked with 5% bovine serum albumin (BSA) and incubated 1 h at room temperature with integrin-β1 antibody (Abcam). Alexa fluor 488 (Invitrogen, Life Technologies, NY, USA) was used as secondary antibody. Images were acquired on a Leica TCS SP5II confocal microscope (Leica Microsystems) using a Plan-Apochromat 63× oil objective. Images were processed using the LAS AF software (Leica Microsystems). Background noise was minimal when optimal gain/offset settings for the detectors were used. Digital images were optimized for contrast and brightness using Adobe Photoshop (Adobe Systems, San Jose, USA).

### Adhesion assay

Cell adhesion assay was performed in 96-well plates, previously coated with fibronectin, type-I or type-IV collagen (all from Sigma-Aldrich) (5 μg/ml) overnight at 4°C. Plates were washed three times in PBS and non-specific-binding sites were blocked by adding 0.5% BSA (w/v) in PBS containing Pen/Strep for 2 h at 37°C. A total volume of 100 μl serum-free medium, containing $10^6$ cells/ml, was plated in coated wells for 30 min, after which plates were washed with PBS to remove non-adherent cells, and the attached cells were fixed with acetone : methanol (1 : 1) for 10 min at 4°C. Cell adhesion was determined following the colorimetric method described by Busk *et al.* (47). The absorbance was measured at 570 nm with a microplate reader. The attachment of cells to wells coated with 1 mg/ml of poly-L-Lys and fixed with 4% paraformaldehyde before aspiration was defined as 100% of adhesion.

### Imaging flow cytometry

To characterize the integrin-β1 and integrin-α5β1 distribution by imaging flow cytometry, $10^6$ cells were seeded for 24 h, detached with Versene (GIBCO) and processed as live cells in suspension. Cells were incubated with integrin-β1 (Abcam) and integrin-α5β1 (Merck Millipore, Billerica, USA) antibodies for 1 h at room temperature. Alexa fluor 488 (Invitrogen) was used as the secondary antibody. Samples were analysed in the imaging flow cytometer (ImageStream®, Amnis, EDM Millipore), using a 488 nm excitation laser. All images were captured with the 40× objective (image pixel 0.5 $\mu m^2$) using the INSPIRE software (Amnis, EDM Millipore), acquiring at least 10 000 events.

Data were analysed using the IDEAS® software (Amnis, EDM Millipore, version 6.0.348) using only the single cell events. For the quantification of the fluorescence intensity of the labelled integrin-β1/integrin-α5β1 in the plasma membrane, a mask fitting the plasma membrane was built using the corresponding bright-field image, and fluorescence intensity was quantified within this region of interest.

### Phenformin treatments

The effect of phenformin (Sigma-Aldrich) over respiration was evaluated by adding 5 mM phenformin before CCCP or oligomycin in oxygen consumption experiments described above. For confocal microscopy or imaging flow cytometry, 5 mM phenformin was added 1 h before fixation or cell harvesting, respectively.

### Xenografts

All the procedures were carried out in accordance with the Guidelines for the Care and Use of Laboratory Animals, directive 86/609/EEC. N:NIH(s)II:nu/nu nude mice were subcutaneously injected in the dorsal flanks with $10^6$ cells of WT or tRNAmut cybrids. Mouse weight and tumour width and length were measured with callipers every week. Excised tumours and lungs (to assess the presence of metastases) were fixed with 4% neutral buffered formalin and paraffin-embedded. The presence of lung metastases was evaluated by immunohistochemistry using anti-vimentin monoclonal antibody (DAKO, Glostrup, USA), and the streptavidin–biotin–horseradish peroxidase technique.

### Statistical analysis

Statistical analysis was performed using GraphPad software (GraphPad Software Inc., La Jolla, USA), using Student's *t*-test or two-way ANOVA with Tukey *post hoc* test. Differences were considered statistically significant when $P < 0.05$ ($^*P < 0.05$; $^{**}P < 0.01$; $^{***}P < 0.001$).

## Acknowledgements

We thank Nuno Mendes and Adriana Gaspar da Rocha for their excellent support in animal handling and tissue processing.

*Conflict of Interest statement*. None declared.

## Funding

This work was supported by Fundação para a Ciência e Tecnologia through PhD grant SFRH/BD/90124/2012 (J.B.N), Program Ciência 2007 (V.M.) and Program Ciência 2008 (J.L.). Further funding was obtained from the project 'Microenvironment, metabolism and cancer' based at IPATIMUP and partially supported by Programa Operacional Regional do Norte (ON. 2—O Novo Norte), under the Quadro de Referência Estratégico Nacional (QREN) and through the Fundo Europeu de Desenvolvimento Regional (FEDER). IPATIMUP is an Associate Laboratory of the Portuguese Ministry of Science, Technology and Higher Education that is partially supported by the FCT. Research in KKS Laboratory is supported by Veterans Administration grant 1I01BX001716.

## References

1. Vander Heiden, M.G., Cantley, L.C. and Thompson, C.B. (2009) Understanding the Warburg effect: the metabolic requirements of cell proliferation. *Science*, **324**, 1029–1033.
2. DeBerardinis, R.J., Lum, J.J., Hatzivassiliou, G. and Thompson, C.B. (2008) The biology of cancer: metabolic reprogramming fuels cell growth and proliferation. *Cell Metab.*, **7**, 11–20.
3. Warburg, O. (1956) On the origin of cancer cells. *Science*, **123**, 309–314.
4. Warburg, O., Wind, F. and Negelein, E. (1927) The metabolism of tumors in the body. *J. Gen. Physiol.*, **8**, 519–530.
5. Koppenol, W.H., Bounds, P.L. and Dang, C.V. (2011) Otto Warburg's contributions to current concepts of cancer metabolism. *Nat. Rev. Cancer*, **11**, 325–337.
6. Wallace, D.C. (2012) Mitochondria and cancer. *Nat. Rev. Cancer*, **12**, 685–698.

7. Maximo, V., Lima, J., Soares, P. and Sobrinho-Simoes, M. (2009) Mitochondria and cancer. *Virchows Arch.*, **454**, 481–495.
8. Simonnet, H., Alazard, N., Pfeiffer, K., Gallou, C., Beroud, C., Demont, J., Bouvier, R., Schagger, H. and Godinot, C. (2002) Low mitochondrial respiratory chain content correlates with tumor aggressiveness in renal cell carcinoma. *Carcinogenesis*, **23**, 759–768.
9. Lievre, A., Chapusot, C., Bouvier, A.M., Zinzindohoue, F., Piard, F., Roignot, P., Arnould, L., Beaune, P., Faivre, J. and Laurent-Puig, P. (2005) Clinical value of mitochondrial mutations in colorectal cancer. *J. Clin. Oncol.*, **23**, 3517–3525.
10. Larman, T.C., DePalma, S.R. and Hadjipanayis, A.G., Cancer Genome Atlas Research Network, Protopopov, A., Zhang, J., Gabriel, S.B., Chin, L., Seidman, C.E., Kucherlapati, R. *et al.* (2012) Spectrum of somatic mitochondrial mutations in five cancers. *Proc. Natl Acad. Sci. USA*, **109**, 14087–14091.
11. Imanishi, H., Hattori, K., Wada, R., Ishikawa, K., Fukuda, S., Takenaga, K., Nakada, K. and Hayashi, J. (2011) Mitochondrial DNA mutations regulate metastasis of human breast cancer cells. *PLoS One*, **6**, e23401.
12. Ishikawa, K., Takenaga, K., Akimoto, M., Koshikawa, N., Yamaguchi, A., Imanishi, H., Nakada, K., Honma, Y. and Hayashi, J. (2008) ROS-generating mitochondrial DNA mutations can regulate tumor cell metastasis. *Science*, **320**, 661–664.
13. Hood, J.D. and Cheresh, D.A. (2002) Role of integrins in cell invasion and migration. *Nat. Rev. Cancer*, **2**, 91–100.
14. King, M.P. and Attardi, G. (1989) Human cells lacking mtDNA: repopulation with exogenous mitochondria by complementation. *Science*, **246**, 500–503.
15. Shaag, A., Saada, A., Steinberg, A., Navon, P. and Elpeleg, O.N. (1997) Mitochondrial encephalomyopathy associated with a novel mutation in the mitochondrial tRNA(leu)(UUR) gene (A3243 T). *Biochem. Biophys. Res. Commun.*, **233**, 637–639.
16. Gasparre, G., Kurelac, I., Capristo, M., Iommarini, L., Ghelli, A., Ceccarelli, C., Nicoletti, G., Nanni, P., De Giovanni, C., Scotlandi, K. *et al.* (2011) A mutation threshold distinguishes the antitumorigenic effects of the mitochondrial gene MTND1, an oncojanus function. *Cancer Res.*, **71**, 6220–6229.
17. Lu, P., Weaver, V.M. and Werb, Z. (2012) The extracellular matrix: a dynamic niche in cancer progression. *J. Cell Biol.*, **196**, 395–406.
18. Ganguly, K.K., Pal, S., Moulik, S. and Chatterjee, A. (2013) Integrins and metastasis. *Cell Adh. Migr.*, **7**, 251–261.
19. Smith, J.C., Symes, K., Hynes, R.O. and DeSimone, D. (1990) Mesoderm induction and the control of gastrulation in *Xenopus laevis*: the roles of fibronectin and integrins. *Development*, **108**, 229–238.
20. Gu, J. and Taniguchi, N. (2004) Regulation of integrin functions by N-glycans. *Glycoconj. J.*, **21**, 9–15.
21. Isaji, T., Sato, Y., Fukuda, T. and Gu, J. (2009) N-glycosylation of the I-like domain of beta1 integrin is essential for beta1 integrin expression and biological function: identification of the minimal N-glycosylation requirement for alpha5beta1. *J. Biol. Chem.*, **284**, 12207–12216.
22. Janik, M.E., Litynska, A. and Vereecken, P. (2010) Cell migration—the role of integrin glycosylation. *Biochim. Biophys. Acta*, **1800**, 545–555.
23. Owen, M.R., Doran, E. and Halestrap, A.P. (2000) Evidence that metformin exerts its anti-diabetic effects through inhibition of complex 1 of the mitochondrial respiratory chain. *Biochem. J.*, **348**, 607–614.
24. Polyak, K., Li, Y., Zhu, H., Lengauer, C., Willson, J.K., Markowitz, S.D., Trush, M.A., Kinzler, K.W. and Vogelstein, B. (1998) Somatic mutations of the mitochondrial genome in human colorectal tumours. *Nat. Genet.*, **20**, 291–293.
25. Maximo, V., Soares, P., Lima, J., Cameselle-Teijeiro, J. and Sobrinho-Simoes, M. (2002) Mitochondrial DNA somatic mutations (point mutations and large deletions) and mitochondrial DNA variants in human thyroid pathology: a study with emphasis on Hurthle cell tumors. *Am. J. Pathol.*, **160**, 1857–1865.
26. Maximo, V., Soares, P., Machado, J.C., Seruca, R. and Sobrinho-Simoes, M. (2000) Mitochondrial DNA alteration in gastric cancer. *Gastroenterology*, **119**, 1808–1809.
27. Li, L.H., Kang, T., Chen, L., Zhang, W., Liao, Y., Chen, J. and Shi, Y. (2014) Detection of mitochondrial DNA mutations by high-throughput sequencing in the blood of breast cancer patients. *Int. J. Mol. Med.*, **33**, 77–82.
28. Jeronimo, C., Nomoto, S., Caballero, O.L., Usadel, H., Henrique, R., Varzim, G., Oliveira, J., Lopes, C., Fliss, M.S. and Sidransky, D. (2001) Mitochondrial mutations in early stage prostate cancer and bodily fluids. *Oncogene*, **20**, 5195–5198.
29. Meierhofer, D., Mayr, J.A., Fink, K., Schmeller, N., Kofler, B. and Sperl, W. (2006) Mitochondrial DNA mutations in renal cell carcinomas revealed no general impact on energy metabolism. *Br. J. Cancer*, **94**, 268–274.
30. Lorenc, A., Bryk, J., Golik, P., Kupryjanczyk, J., Ostrowski, J., Pronicki, M., Semczuk, A., Szolkowska, M. and Bartnik, E. (2003) Homoplasmic MELAS A3243G mtDNA mutation in a colon cancer sample. *Mitochondrion*, **3**, 119–124.
31. Petros, J.A., Baumann, A.K., Ruiz-Pesini, E., Amin, M.B., Sun, C. Q., Hall, J., Lim, S., Issa, M.M., Flanders, W.D., Hosseini, S.H. *et al.* (2005) mtDNA mutations increase tumorigenicity in prostate cancer. *Proc. Natl Acad. Sci. USA*, **102**, 719–724.
32. Shidara, Y., Yamagata, K., Kanamori, T., Nakano, K., Kwong, J. Q., Manfredi, G., Oda, H. and Ohta, S. (2005) Positive contribution of pathogenic mutations in the mitochondrial genome to the promotion of cancer by prevention from apoptosis. *Cancer Res.*, **65**, 1655–1663.
33. Kulawiec, M., Owens, K.M. and Singh, K.K. (2009) Cancer cell mitochondria confer apoptosis resistance and promote metastasis. *Cancer Biol. Ther.*, **8**, 1378–1385.
34. Kwong, J.Q., Henning, M.S., Starkov, A.A. and Manfredi, G. (2007) The mitochondrial respiratory chain is a modulator of apoptosis. *J. Cell Biol.*, **179**, 1163–1177.
35. He, X., Zhou, A., Lu, H., Chen, Y., Huang, G., Yue, X., Zhao, P. and Wu, Y. (2013) Suppression of mitochondrial complex I influences cell metastatic properties. *PLoS One*, **8**, e61677.
36. van Waveren, C., Sun, Y., Cheung, H.S. and Moraes, C.T. (2006) Oxidative phosphorylation dysfunction modulates expression of extracellular matrix—remodeling genes and invasion. *Carcinogenesis*, **27**, 409–418.
37. Pinho, S.S., Carvalho, S., Marcos-Pinto, R., Magalhaes, A., Oliveira, C., Gu, J., Dinis-Ribeiro, M., Carneiro, F., Seruca, R. and Reis, C.A. (2013) Gastric cancer: adding glycosylation to the equation. *Trends Mol. Med.*, **19**, 664–676.
38. Pinho, S.S., Figueiredo, J., Cabral, J., Carvalho, S., Dourado, J., Magalhaes, A., Gartner, F., Mendonfa, A.M., Isaji, T., Gu, J. *et al.* (2013) E-cadherin and adherens-junctions stability in gastric carcinoma: functional implications of glycosyltransferases involving N-glycan branching biosynthesis, N-acetylglucosaminyltransferases III and V. *Biochim. Biophys. Acta*, **1830**, 2690–2700.
39. Wang, L., Liang, Y., Li, Z., Cai, X., Zhang, W., Wu, G., Jin, J., Fang, Z., Yang, Y. and Zha, X. (2007) Increase in beta1-6 GlcNAc branching caused by N-acetylglucosaminyltransferase V directs integrin beta1 stability in human hepatocellular carcinoma cell line SMMC-7721. *J. Cell Biochem.*, **100**, 230–241.

40. Asada, M., Furukawa, K., Segawa, K., Endo, T. and Kobata, A. (1997) Increased expression of highly branched *N*-glycans at cell surface is correlated with the malignant phenotypes of mouse tumor cells. *Cancer Res.*, **57**, 1073–1080.
41. Sasai, K., Ikeda, Y., Fujii, T., Tsuda, T. and Taniguchi, N. (2002) UDP-GlcNAc concentration is an important factor in the biosynthesis of beta1,6-branched oligosaccharides: regulation based on the kinetic properties of *N*-acetylglucosaminyltransferase V. *Glycobiology*, **12**, 119–127.
42. Mullen, A.R., Wheaton, W.W., Jin, E.S., Chen, P.H., Sullivan, L. B., Cheng, T., Yang, Y., Linehan, W.M., Chandel, N.S. and DeBerardinis, R.J. (2012) Reductive carboxylation supports growth in tumour cells with defective mitochondria. *Nature*, **481**, 385–388.
43. Wellen, K.E., Lu, C., Mancuso, A., Lemons, J.M., Ryczko, M., Dennis, J.W., Rabinowitz, J.D., Coller, H.A. and Thompson, C.B. (2010) The hexosamine biosynthetic pathway couples growth factor-induced glutamine uptake to glucose metabolism. *Genes Dev.*, **24**, 2784–2799.
44. Hung, W.Y., Huang, K.H., Wu, C.W., Chi, C.W., Kao, H.L., Li, A. F., Yin, P.H. and Lee, H.C. (2012) Mitochondrial dysfunction promotes cell migration via reactive oxygen species-enhanced beta5-integrin expression in human gastric cancer SC-M1 cells. *Biochim. Biophys. Acta*, **1820**, 1102–1110.
45. Saffran, H.A., Pare, J.M., Corcoran, J.A., Weller, S.K. and Smiley, J.R. (2007) Herpes simplex virus eliminates host mitochondrial DNA. *EMBO Rep.*, **8**, 188–193.
46. Chomyn, A. (1996) Platelet-mediated transformation of human mitochondrial DNA-less cells. *Methods Enzymol.*, **264**, 334–339.
47. Busk, M., Pytela, R. and Sheppard, D. (1992) Characterization of the integrin alpha v beta 6 as a fibronectin-binding protein. *J. Biol. Chem.*, **267**, 5790–5796.